Available online at www.eccomasproceedia.org
Eccomas Proceedia COMPDYN (2023) 1126-1137

ECCOMAS
Proceedia

COMPDYN 2023
9th ECCOMAS Thematic Conference on
Computational Methods in Structural Dynamics and Earthquake Engineering
M. Papadrakakis, M. Fragiadakis (eds.)
Athens, Greece, 12-14 June 2023

A METHODOLOGY FOR THE EVALUATION OF MORPHOLOGY-BASED CONSTITUTIVE LAWS OF CORRODED STEEL REBARS

F. Di Carlo[1], D.A. Talledo[2], L. Berto[2], P. Isabella[1], A. Meda[1], Z. Rinaldi[1], I. Rocca[2] and A. Saetta[2]

[1] DICII - University of Rome "Tor Vergata"
Via del Politecnico 1, 00133 Rome, Italy
{di.carlo,rinaldi}@ing.uniroma2.it, {alberto.meda,paolo.isabella}@uniroma2.it

[2] DCP- University IUAV of Venice
Dorsoduro 2206, Venice 30123, Italy
{dtalledo,luisa.berto,irocca,saetta}@iuav.it

Abstract

The assessment of degraded reinforced concrete (RC) existing structures is nowadays a topical problem since several ones have an age close to or higher than their design life. The degradation state of the structure needs to be properly assessed and included in the adopted numerical or analytical models. In this framework, rebars corrosion phenomena can modify the structural behavior of RC members, especially when the corrosive attack is localized in specific areas. As an example, in presence of localized concentrations of chlorides, pitting corrosion of the steel bars occurs, with a localized reduction of the bar section through pits. In this work, the results of a preliminary experimental survey performed on artificially corroded steel rebars are shown, to define an integrated methodology for the definition of material constitutive laws, accounting for morphological aspects of the corrosion phenomenon. A set of steel rebars, embedded in concrete prisms, have been artificially corroded with an accelerated process through electrolytic cells, to obtain local marked pits. The steel rebars have been extracted, cleaned, weighed and subjected to 3D scanning using two different techniques (one based on laser scanning and the other based on structured-light scanning) to evaluate the effective corrosion amount and morphology. Finally, tensile tests were carried out to evaluate the stress-strain curves and the values of yielding, ultimate strengths and elongation to fracture. The presented data and methodology can represent a useful reference for the definition of phenomenological constitutive laws for steel rebars affected by pitting corrosion.

Keywords: Corrosion, Steel rebars, Morphology, 3D Scanning, Constitutive laws.

ISSN:2623-3347
Peer-review under responsibility of the organizing committee of COMPDYN 2023.
doi: 10.7712/120123.10463.21356

1 INTRODUCTION

Corrosion of the steel reinforcement is one of the main causes of degradation in reinforced concrete (RC) structures, especially when the corrosive attack is localized in specific areas and pitting corrosion occurs. Corrosion phenomena are generally responsible for a reduction of the cross section of the steel rebars and a decrease of the yielding and ultimate strengths and of the ultimate strain. A proper assessment of the mechanical properties of corroded steel rebars is thus fundamental when evaluating the residual performance of concrete structures through numerical or analytical models. Nevertheless, the study of the influence of corrosion on the reinforcing steel mechanical properties is nowadays an open research issue, as witnessed by the wide recent literature both on artificially and naturally corroded steel rebars.

In [1] the results of an experimental study on the static tensile and fatigue behavior of corroded bars are reported. Tensile tests of high ductility reinforcements with different corrosion levels are described in [2]. An investigation on the behavior of Tempcore rebars damaged by a local abrasion, to simulate the effect of pitting corrosion, is described in [3]. An experimental investigation into the tensile behaviour of corroded steel bars under different strain rates is reported in [4]. Degradation equations for the mechanical properties of corroded steel rebars, based on the results of experimental tests on artificially deteriorated rebars, with different diameters and subjected to different corrosion degrees, can be found in [5]. In [6] the results of tensile and low-cycle fatigue tests on different typologies of steel bars representative of the European production scenario are reported. The outcomes of tensile tests performed on 16 mm B500B ribbed bars, locally damaged by using a CNC milling machine can be found in [7]. The authors also propose new relationships for the estimation of the residual mechanical properties of the corroded reinforcement. Experimental tests on three duplex stainless steel (DSS) bars embedded in concrete exposed to natural chloride penetration are described in [8]. A comparison between the performance of Dual-Phase and Tempcore rebars in uncorroded and corroded conditions is reported in [9]. In [10] the results of uniaxial tensile tests combined with the Digital Image Correlation technique on 61 rebars taken pre- and un- cracked RC beams subjected to drying and wetting cycles in chloride solution for over three years are presented.

With reference to naturally corroded steel rebars, various researches can be found in literature. In [11] an experimental investigation on samples of steel rebars extracted from coastal buildings in Greece up to 96 years old is described, finding a serious degradation of the material and its mechanical properties. The results of mechanical experiments conducted on corroded bars retrieved from RC beams exposed to a chloride environment for 26 and 28 years are shown in [12]. In [13] a 4-year natural corrosion experiment on corroded bars in pre-cracked RC elements is described. In [14] the mechanical properties of naturally corroded reinforcement buried for 60 years are analyzed. A comparison between naturally and artificially corroded rebars can be found in [15] and [16].

A number of literature papers present 3D scanning of rebars carried out with different techniques and different aims. In [17] the authors used structured light 3D scanner on 23 corroded bars, trying to determine some statistical measures able to describe the pit corrosion morphology. In [18] it is reported a study on 13 reinforced concrete beams subjected to natural corrosion with an exposition of more than 30 years. The study aimed at finding correlations between the crack widths and corrosion level, proposing a damage indicator based on the crack width that can be measured from in-situ inspections. In [19] the focus was on the study of local effects of pits on the corroded mechanical properties derived by cyclic and monotonic tests; furthermore the authors proposed a fibre-based model for fast-simulation of mechanical properties of corroded steel bars. In [20] the authors focused on the flexural behavior of corroded beams made of fibre-reinforced concrete, while in [21] there is an interesting comparison of different

cleaning methods (i.e. metallic brushing, acid immersion and sandblasting) for rust removal. In [22] the authors aimed at defining constitutive law for pitting-corroded prestressing steel strands by comparison of 3d scanning and tensile tests performed on naturally corroded steel strands.

The present paper describes the results of a preliminary experimental survey performed on artificially corroded steel rebars, useful to define an integrated methodology, illustrated in Section 2, for the definition of stress-strain laws accounting for morphological aspects of the corrosion phenomenon. Section 3 addresses the various phases of the experimental campaign, including a set of steel rebars, embedded in concrete prisms, artificially corroded with an accelerated process through electrolytic cells, to obtain local marked pits. After the corrosion process the steel rebars have been extracted, cleaned and weighed. Then the steel rebars have been subjected to 3D scanning using two different techniques, a first one based on laser scanning and a second one based on structured-light scanning. The comparison between these two technologies has been performed with the aim to evaluate the effective corrosion amount and morphology, taking into account the precision of the measures which should be always evaluated. Finally, tensile tests have been carried out to evaluate the stress-strain curves and the degradation of the mechanical properties with the main parameters of the corrosion phenomenon. With reference to the above principal phases, the main results of the experimental survey are presented in Section 4.

2 METHODOLOGY

The proposed approach for the definition of phenomenological constitutive laws for steel rebars affected by pitting corrosion is based on the exploitation of the results of experimental tests performed on artificially corroded rebars. A flow chart of the proposed methodology is given in Figure 1, where six different and subsequent phases can be identified:

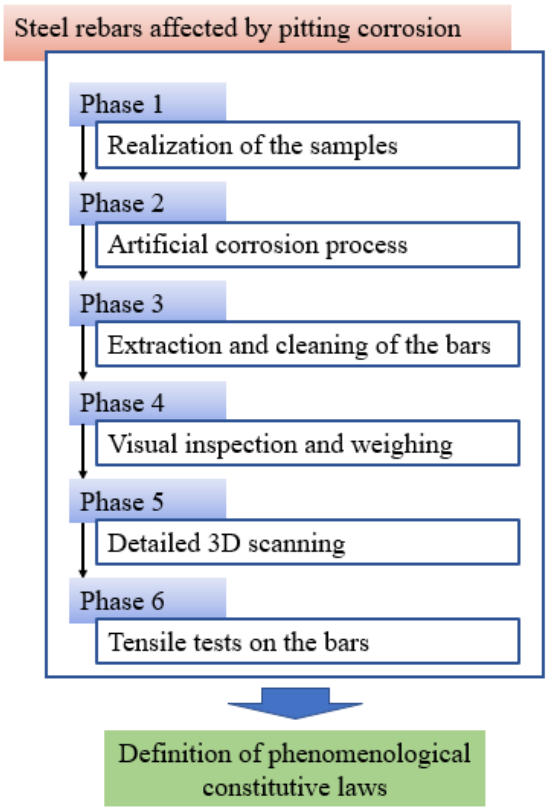

Figure 1: Flow chart of the proposed methodology.

1. Phase 1: realization of the samples, consisting in a steel rebar embedded in a concrete prism;
2. Phase 2: execution of the artificial corrosion process through electrolytic cells, by dipping the concrete prisms within a 3% saline solution;
3. Phase 3: extraction and cleaning of the steel rebars
4. Phase 4: preliminary evaluation of the effective corrosion amount and morphology through visual inspection and weighing of the rebars;
5. Phase 5: assessment of the effective corrosion amount and morphology through the execution of detailed 3D scanning of the bars;
6. Phase 6: execution of tensile tests for the evaluation of the stress-strain relationships of the rebars and the values of yield and ultimate strengths, as well as the elongation to fracture.

3 EXPERIMENTAL CAMPAIGN

The proposed methodology, described in Section 2, has been applied in an experimental survey on steel rebars with a diameter equal to 16 mm. In particular, one steel rebar has been kept un-corroded for reference, while seven rebars have been embedded in concrete prisms and subjected to an artificial corrosion process, to obtain local marked pits. Table 1 shows the layout of the experimental program, together with the investigated parameters of the corrosion process. Three values of the forecast mass loss have been considered, equal to 15%, 20% and 25%. Furthermore, three values of the current density have been adopted, equal to 250, 500 and 800 $\mu A/cm^2$, respectively. The first two values fall within the range available in literature and considered still acceptable for the study of phenomena not involving an interaction with concrete. The last one, out of the recommended range, has been specially chosen to evaluate possible differences in the outcomes of the corrosion process. The experimental tests have been performed at the Laboratory of the University of Rome "Tor Vergata", while the detailed 3D scanning of the rebars has been executed at the University IUAV of Venice.

Specimen	Corroded Length [mm]	Forecast Mass Loss [%]	Current Density [$\mu A/cm^2$]	Current Intensity [A]	Measured Mass Loss [%]
UC	-	-	-	-	-
C5	353	15	250	0.044	17.8
C6	369	15	500	0.093	18.2
C3	338	20	250	0.042	18.4
C1	340	20	500	0.085	18.4
C2	266	25	250	0.033	28.7
C4	279	25	500	0.070	26.3
C0	340	25	800	0.137	24.2

Table 1: Experimental program.

3.1 Geometry of the specimens

The realized concrete samples feature a prismatic shape, with a rectangular 150 mm x 130 mm cross section and a length equal to the corroded length of the rebar, shown in Table 1 and variable in the range between 260 mm and 370 mm. The minimum value of the concrete cover of the embedded steel rebar varies between 30 mm and 50 mm. As shown in Figure 2,

each specimen is characterized by two external portions of steel bar, each one coming out of the bases of the concrete prism for a length of about 100 mm.

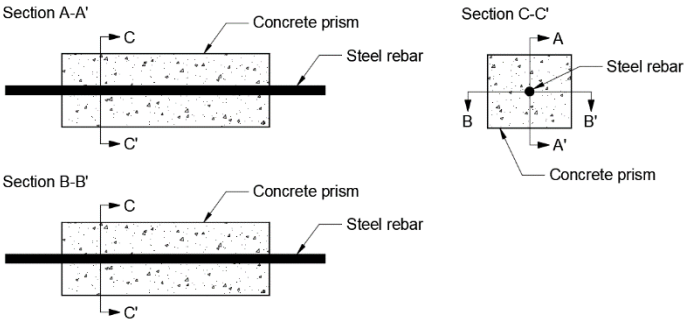

Figure 2: Geometry of the specimens.

3.2 Artificial corrosion process

The artificial corrosion has been provided with an accelerated process through electrolytic cells, by completely dipping the concrete prisms within a 3% saline solution. Each specimen has been placed in a plastic box, on small plastic supports in order to ensure the exposure to the saline solution in all sides of the element. One of the two portions of the steel rebar external to each sample has been connected to the positive pole of a dedicated power supply (anode). The cathodes have been realized with steel bars soaked in the saline solution. Figure 3 shows the scheme of the system adopted to accelerate the corrosion process and some images of the specimens inside the plastic box. As shown in Figure 3, both rebar portions external to the concrete prism have been properly sealed with plastic pipes, to avoid corrosion in these parts, representing the grip length required for the tensile tests.

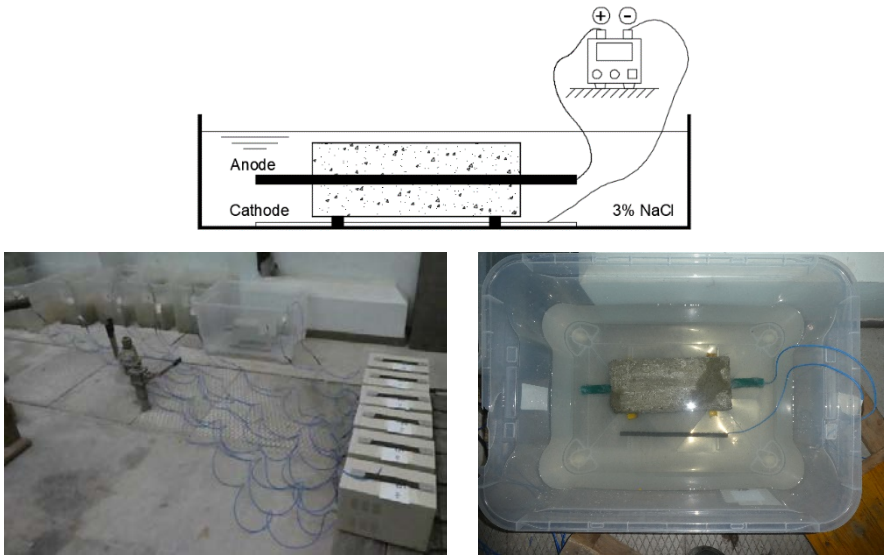

Figure 3: Scheme and images of the system adopted for the accelerated corrosion process.

The required time for obtaining the desired corrosion level, equal to 15% in mass loss, was evaluated with the Faraday's law, suitably modified in order to account for the concrete presence:

$$time[\text{sec}] = \frac{\lambda \cdot m_{loss} \cdot n_{specimen} \cdot C_{Faraday}}{current[A] \cdot M_{specimen}} \quad (1)$$

where m_{loss} is the forecast mass loss, *current* is the current intensity, $M_{specimen}$ is the molar mass of the reinforcing rebar (equal to 55.8 g/mol), $n_{specimen}$ is the valence equal to 2, $C_{Faraday}$ is the Faraday constant (equal to 96485 C/mol) and λ is the constant accounting for the possibility that the corrosive process does not start immediately due to the concrete cover, assumed equal to 1.1, due to the poor quality of the concrete material.

3.3 3D scanning setup

The phase of 3D scanning process can be carried out with different technologies. One of the main issues of this phase is related to the precision of the measures.

First, the scanning was performed with a relatively low-cost structured light 3D scanner (HP scanner 3D pro S3) on the first experimentally corroded bar (i.e. sample C0, with a high current density of 800 μA/cm^2). From the acquisition it was evident that the measure errors (when compared with manual measures by means of a caliber on the real specimen) were of the same order of magnitude of the corrosion process, with errors (in some regions of the bar) up to about 1.5-2.0 mm.

For this reason, the scanning process for all the bars was performed with two different more reliable devices and setups, permitting to compare the results and to estimate the difference of the measures between the two techniques. A first scan was performed with a Range 7 Konica Minolta structured light 3D scanner with a declared accuracy of about 40 μm. The bar was set in vertical position using a clamp adapted with an ad-hoc 3d printed support. The bar is rotated manually with an angle of about 30°-40° during the acquisition, to scan the whole surface. Then the 3D model is generated with the proprietary software of the scanner aligned aligning all the scanned surfaces. Finally, the STL file is generated for each bar. The scanning setup with structured light is depicted in Figure 4.

A second scan was performed with a top state-of-the-art laser scanner FARO® Quantum S mounted on a 8-axis robotic arm. This setup is specifically devoted to metrology testing and inspection and with a certified accuracy of about 50 μm. A specifically designed clamp for the bars was 3D printed allowing a correct positioning and vertical alignment of the bar, subsequently the clamp was mounted and calibrated on the 8th axis of the scan-arm. The scan was performed in two steps in order to obtain a model of the whole bar since for each scan the part covered by the support was not visible. Then the model was constructed by aligning the two scans with a best-fit procedure. Finally, the STL file is generated for each bar. Figure 5 depicts the setup adopted for the laser scanning.

Figure 4: structured light 3d scanning setup.

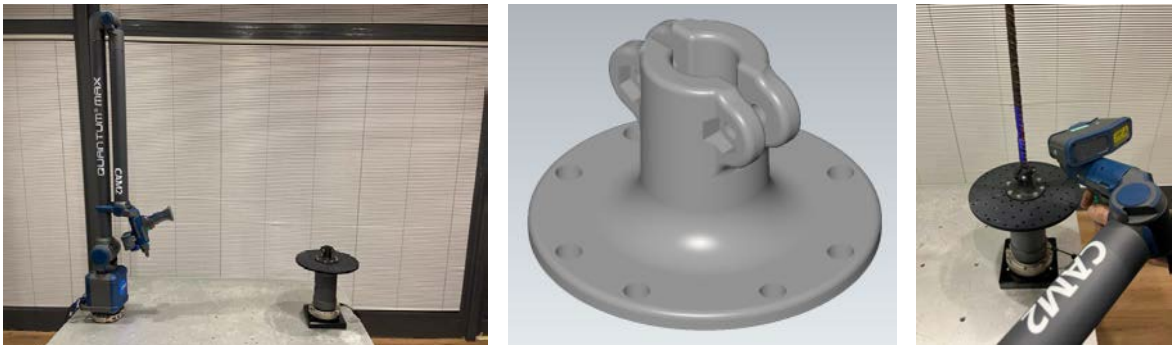

(a) (b) (c)

Figure 5: a) laser scanning setup; b) model of the 3D printed clamp; c) phase of scanning.

3.4 Tensile tests set-up

The tensile tests have been conducted on a 600 kN testing machine, as shown in Figure 6. The applied load has been measured with a load transducer, while a potentiometer transducer has been placed on the steel rebar, at its most probable failure zone, including the sections characterized by the more marked pits. The load value has been used to calculate the stress, based on the nominal cross-sectional area of the rebar before corrosion. The strain has been evaluated as the average strain within the potentiometer transducer length, equal to 200 mm. The performed tests allow obtaining the stress-strain curve of the rebar, together with the values of the yielding and ultimate strengths, f_y and f_u, respectively, as well as the elongation to fracture ε_u.

Figure 6: Tensile test set-up and details of the potentiometer transducer positioning.

4 RESULTS AND DISCUSSIONS

4.1 Visual inspection and weighing

After the artificial corrosion process, the steel rebars have been extracted from the specimens and the actual corrosion has been evaluated in terms of mass loss, by weighing the reinforcement after the rebar cleaning in agreement with [23]. The actual mass loss values are summarized in the last column of Table 1 for each specimen. Figure 7 shows the corroded rebars, together with some details of the sections characterized by the occurrence of the more marked pits. It is highlighted that specimens *C5*, *C6*, *C1* and *C3*, for which a similar value of the

measured mass loss percentage is found, equal to about 18%, feature a substantially different corrosion pattern, resulting in local pits more and more marked. Furthermore, more pronounced pits are found with increasing current density, except for the rebar *C1*. Finally, it is highlighted that in the specimen *C0*, having the highest value of current density, a corrosion pattern characterized by a continuous notch along the longitudinal direction of the rebar is found.

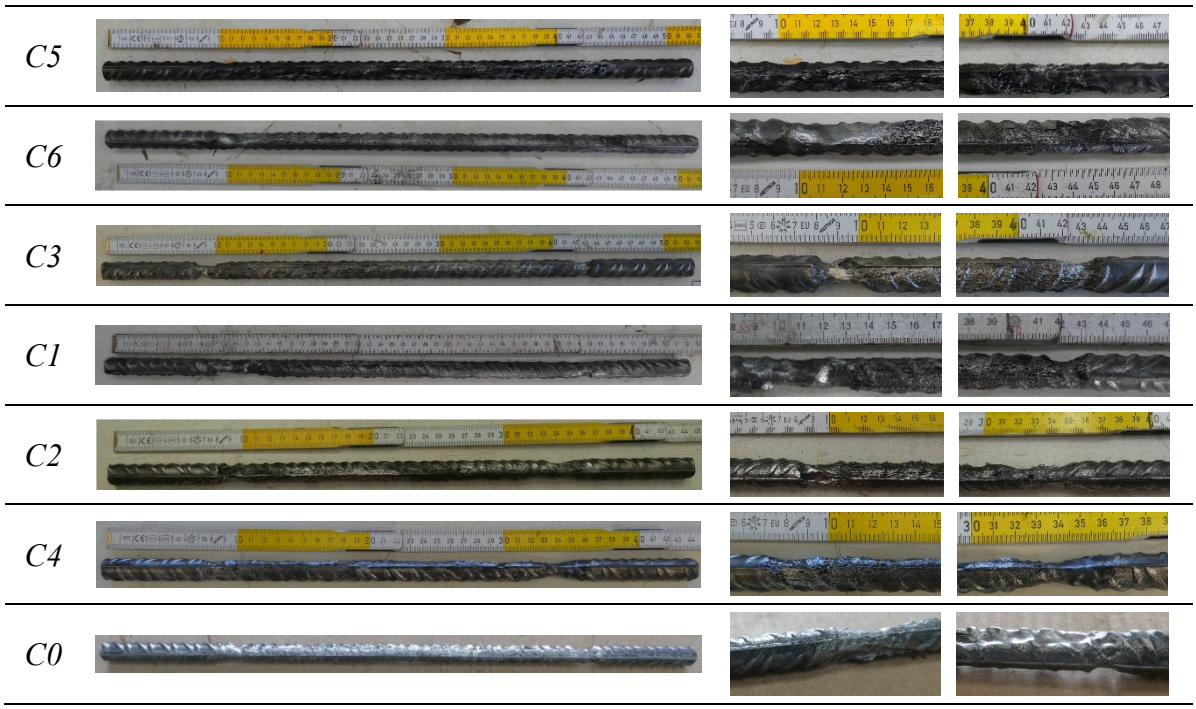

Figure 7: Details of the steel rebars extracted after the corrosion process.

4.2 3D scanning

The models obtained with the two techniques have been imported in the software Polyworks for a comparison of the results obtained. As an example, for the specimens C1 and C2 Figure 8 shows the profiles of the measured difference between the models obtained with structured light and the models obtained with laserscan, assumed as reference due to the certified accuracy reached and the certification of calibration of the instrument used. For all the samples, Table 2 summarizes the statistics of the errors of the measures obtained from structured light with respect to those obtained from the reference laserscan technology (i.e. average error μ, standard deviation σ, maximum and minimum errors).

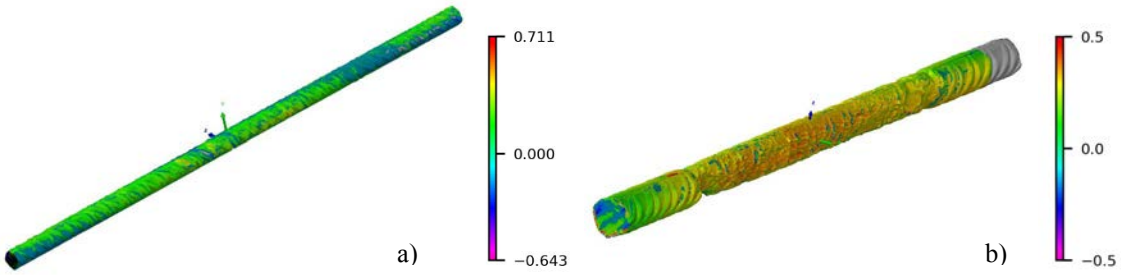

Figure 8: Profile difference (mm) between the models obtained by using structured light and laserscan techniques: a) sample C1, b) sample C2

Specimen	Statistics of errors of structured light and laserscan measures			
	μ (mm)	σ (mm)	max (mm)	min (mm)
UC	0.016	0.093	0.982	-0.993
C5	0.021	0.155	0.851	-0.842
C6	0.040	0.083	0.958	-0.859
C3	0.123	0.150	1.226	-1.230
C1	0.044	0.122	0.711	-0.643
C2	0.145	0.121	1.491	-1.499
C4	0.032	0.083	0.751	-0.675
C0	0.056	0.068	0.901	-0.797

Table 2: Statistics of the errors of the measures obtained from structured light with respect to those obtained from laserscan.

From the previous analyses it is possible to observe that the average difference between the models is lower than 60 μm for the majority of the cases with an average difference above 100 μm just in a couple of samples (i.e. sample C2 and C3). The standard deviation is in the order of 90-150 μm for almost all the samples. The maximum and minimum differences (that happen just in some specific points of the bar, generally the extremities) are less than 1.5 mm in absolute value. Anyhow it is worth noting that the majority of the points (3 standard deviations, corresponding to 99.7% of points) are within a range of ±180-450 μm.

To better assess the pit morphology and distribution for all the samples and in order to define some indexes that can be representative of such aspects, an ad-hoc software tool has been developed to permit the inspection of the whole bar in its cross sections allowing also to measure distances (Figure 9a). Furthermore the software gives a representation of the overall corrosion by means of a 2-D contour map derived from considering each bar with a cylindrical coordinate system aligned with the bar axis (Figure 9b). The alignment in this phase of the research is performed manually with the software Polyworks using the end parts of each sample that are not subjected to corrosion. The software is still under development and will be able to output some descriptive parameters of pitting corrosion along the bar (e.g. corrosion depth, pit area, residual cross area, shape of pit, number and distribution of pits along the sample).

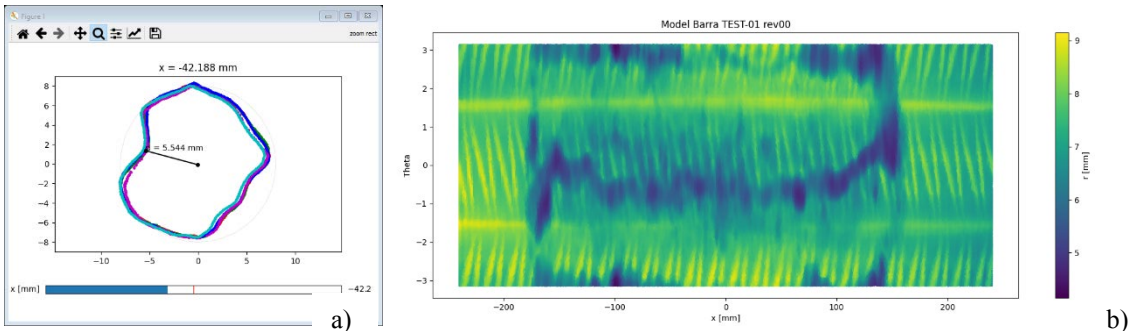

a) b)

Figure 9: Screenshots from developed software tool as an example for bar C0: a) cross sections inspector, b) general corrosion distribution map along the bar

4.3 Tensile tests

Figure 10 shows the results of tensile tests performed on the uncorroded and corroded specimens in terms of stress-strain curve, evaluated with the procedure described in Section 3.4. The curve of the uncorroded specimen UC is indicated with a continuous black line. The ones of the corroded samples are plotted with different colours, varying the forecast mass loss

percentage: green, grey and red colours refer to values of 15%, 20% and 25%, respectively. Vice versa, the style of the curve specifies the adopted current density: continuous, dashed and dotted lines refer to values equal to 250, 500 and 800 μA/cm^2, respectively. A severe reduction of the yielding and ultimate strengths and of the ultimate strain can be observed in the corroded specimens with respect to the uncorroded one, generally increasing with the mass loss percentage. It is worth to highlight that specimens *C5*, *C6*, *C3* and *C1* feature a substantially different behaviour, due to the morphological aspects of corrosion, as previously reported in Section 4.1. Furthermore, for fixed mass loss percentage, a high decrease of the mechanical properties is found with increasing values of the current density (i.e. between continuous and dashed curves), except for the rebar *C3*.

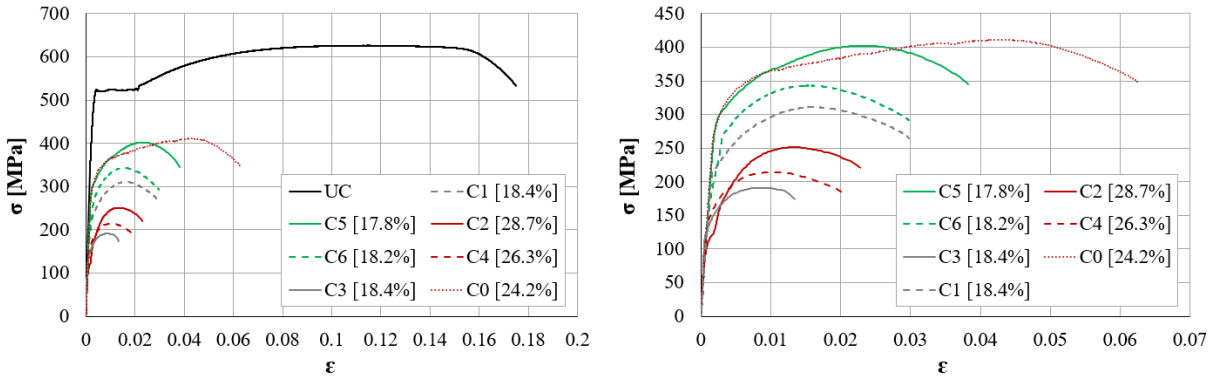

Figure 10: Stress-strain curves: a) uncorroded and corroded rebars; b) corroded rebars.

5 CONCLUSIONS

The preliminary experimental campaign described in the present paper provides a starting point for the definition of an integrated methodology for the evaluation of stress-strain laws of corroded steel rebars, accounting for morphological aspects of the corrosion phenomenon. The proposed procedure is based on a six phases process, consisting of: realization of the samples; execution of the artificial corrosion process; extraction and cleaning of the steel rebars; preliminary evaluation of the effective corrosion amount and morphology through visual inspection and weighing of the rebars; assessment of the effective corrosion amount and morphology through the execution of detailed 3D scanning of the bars; execution of tensile tests. The experimental program has been accurately designed to obtain corrosion layouts characterized by the presence of local marked pits and to investigate some of the most meaningful parameters, among which the average mass loss and current density. The obtained results confirm the importance of the corrosion morphology for the definition of constitutive laws able to properly catch the behaviour of corroded steel rebars. A severe reduction of the yielding and ultimate strengths and of the ultimate strain can be observed in the corroded specimens with respect to the uncorroded one, generally increasing with the mass loss percentage. Nevertheless, the mass loss index alone is not always able to fully describe the investigated problems, since strongly different corrosion pattern, resulting in local pits more and more marked, can be found for the same value of the mass loss. Generally, even if exceptions have been found, more pronounced pits are obtained with increasing current density, with a consequent high decrease of the mechanical properties.

REFERENCES

[1] W. Zhang, X. Song, X. Gu, S. Li, Tensile and fatigue behavior of corroded rebars. *Construction and Building Materials*, **34**, 409-417, 2012.

[2] E. Moreno, A. Cobo, G. Palomo, M.N. González, Mathematical models to predict the mechanical behavior of reinforcements depending on their degree of corrosion and the diameter of the rebars. *Construction and Building Materials*, **61**, 156-163, 2014.

[3] J. Santos, A.A. Henriques, Strength and ductility of damaged Tempcore rebars. *Procedia Engineering*, **114**, 800-807, 2015.

[4] W. Zhang, H. Chen, X. Gu, Tensile behaviour of corroded steel bars under different strain rates. *Magazine of Concrete Research*, **68**(3), 127-140, 2016.

[5] S. Imperatore, Z. Rinaldi, C. Drago, Degradation relationships for the mechanical properties of corroded steel rebars. *Construction and Building Materials*, **148**, 219-230, 2017.

[6] S. Caprili, W. Salvatore, Mechanical performance of steel reinforcing bars in uncorroded and corroded conditions. *Data in Brief*, **18**, 1677-1695, 2018.

[7] I. Finozzi, A. Saetta, H. Budelmann, Structural response of reinforcing bars affected by pitting corrosion: experimental evaluation. *Construction and Building Materials*, **192**, 478-488, 2018.

[8] M.C. Alonso, F.J. Luna, M. Criado, Corrosion behavior of duplex stainless steel reinforcement in ternary binder concrete exposed to natural chloride penetration. *Construction and Building Materials*, **192**, 385-395, 2019.

[9] S. Caprili, W. Salvatore, R. Valentini, C. Ascanio, G. Luvarà, Dual-Phase steel reinforcing bars in uncorroded and corroded conditions. *Construction and Building Materials*, **218**, 162-175, 2019.

[10] E. Chen, C.G. Berrocal, I. Fernandez, I. Löfgren, K. Lundgren, Assessment of the mechanical behaviour of reinforcement bars with localised pitting corrosion by Digital Image Correlation. *Engineering Structures*, **219**, 110936, 2020.

[11] M.P. Papadopoulos, C.A. Apostolopoulos, A.D. Zervaki, G.N. Haidemenopoulos, Corrosion of exposed rebars, associated mechanical degradation and correlation with accelerated corrosion tests. *Construction and Building Materials*, **25**, 3367-3374, 2011.

[12] W. Zhu, R. François, Experimental investigation of the relationships between residual cross-section shapes and the ductility of corroded bars. *Construction and Building Materials*, **69**, 335-345, 2014.

[13] C. Lu, S. Yuan, P. Cheng, R. Liu, Mechanical properties of corroded steel bars in pre-cracked concrete suffering from chloride attack. *Construction and Building Materials*, **123**, 649-660, 2016.

[14] C.E.T. Balestra, M.G. Lima, A.R. Silva, R.A. Medeiros-Junior, Corrosion degree effect on nominal and effective strengths of naturally corroded reinforcement. *Journal of Materials in Civil Engineering*, **28**(10), 04016103, 2016.

[15] Y. Ou, Y.T.T. Susanto, H. Roh, Tensile behavior of naturally and artificially corroded steel bars. *Construction and Building Materials*, **103**, 93-104, 2016.

[16] W. Zhu, R. François, C.S. Poon, J. Dai, Influences of corrosion degree and corrosion morphology on the ductility of steel reinforcement. *Construction and Building Materials*, **148**, 297-306, 2017.

[17] Kashani, M.M., Crewe, A.J., Alexander, N.A., Use of a 3D optical measurement technique for stochastic corrosion pattern analysis of reinforcing bars subjected to accelerated corrosion, *Corrosion Science*, 73, 208-221, 2013

[18] Tahershamsi, M., Fernandez, I., Lundgren, K., Zandi, K., Investigating correlations between crack width, corrosion level and anchorage capacity, *Structure and Infrastructure Engineering*, 2479, 1-14, 2016

[19] Fernandez, I., Bairàn, J.M., Marì, A.R., 3d FEM model development from 3d optical measurement technique applied to corroded steel bars, *Construction and Building Materials*, 124, 519-532, 2016

[20] Berrocal, C.H., Löfgren, I, Lundgren, K., The effect of fibres on steel bar corrosion and flexural behaviour of corroded RC beams, *Engineering Structures*, 163, 15, 409-425, 2018

[21] Fernandez, I., Lundgren, K., Zandi, K., Evaluation of corrosion level of naturally corroded bars using different cleaning methods, computed tomography, and 3D optical scanning, *Materials and Structures*, 62, 78, 2018

[22] Vecchi, F., Franceschini, L., Tondolo, F., Belletti, B., Montero, J.S., Minetola, P., Corrosion morphology of prestressing steel strands in naturally corroded PC beams, *Construction and Building Materials*, 296, 16, 123720, 2021

[23] ASTM G1-90. Practise for preparing, cleaning and evaluating corrosion test specimens. ASTM International, West Conshohocken, Pa, 2002.